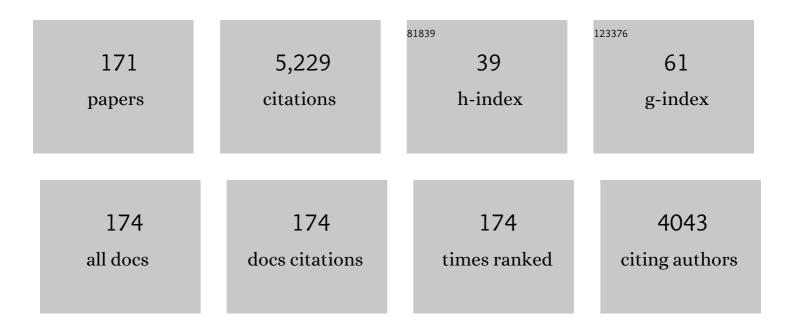
## Angel L Ortiz

List of Publications by Year in descending order

Source: https://exaly.com/author-pdf/3256272/publications.pdf Version: 2024-02-01



ANCEL OPTIZ

#	Article	IF	CITATIONS
1	Composition effects of thermal barrier coating ceramics on their interaction with molten Ca–Mg–Al–silicate (CMAS) glass. Acta Materialia, 2012, 60, 5437-5447.	3.8	208
2	Calcia-magnesia-alumino-silicate (CMAS)-induced degradation and failure of air plasma sprayed yttria-stabilized zirconia thermal barrier coatings. Acta Materialia, 2016, 105, 355-366.	3.8	181
3	Air-plasma-sprayed thermal barrier coatings that are resistant to high-temperature attack by glassy deposits. Acta Materialia, 2010, 58, 6835-6844.	3.8	163
4	X-ray diffraction analysis of a severely plastically deformed aluminum alloy. Acta Materialia, 2004, 52, 2185-2197.	3.8	130
5	2ZrO <sub>2</sub> ·Y <sub>2</sub> O <sub>3</sub> Thermal Barrier Coatings Resistant to Degradation by Molten <scp>CMAS</scp> : Part I, Optical Basicity Considerations and Processing. Journal of the American Ceramic Society, 2014, 97, 3943-3949.	1.9	111
6	Toughening of super-hard ultra-fine grained B4C densified by spark-plasma sintering via SiC addition. Journal of the European Ceramic Society, 2013, 33, 1395-1401.	2.8	110
7	Determination of optical properties in nanostructured thin films using the Swanepoel method. Applied Surface Science, 2006, 252, 6013-6017.	3.1	106
8	Porosity Development in Activated Carbons Prepared from Walnut Shells by Carbon Dioxide or Steam Activation. Industrial & Engineering Chemistry Research, 2009, 48, 7474-7481.	1.8	102
9	Wear-resistant ultra-fine-grained ceramics. Acta Materialia, 2005, 53, 271-277.	3.8	100
10	Influence of preparation conditions in the textural and chemical properties of activated carbons from a novel biomass precursor: The coffee endocarp. Bioresource Technology, 2008, 99, 7224-7231.	4.8	99
11	Densification and porosity evaluation of ZrO2–3 mol.% Y2O3 sol–gel thin films. Thin Solid Films, 2004, 458, 92-97.	0.8	91
12	Interrogation of the microstructure and residual stress of a nickel-base alloy subjected to surface severe plastic deformation. Acta Materialia, 2008, 56, 413-426.	3.8	81
13	Microstructural design of sliding-wear-resistant liquid-phase-sintered SiC: An overview. Journal of the European Ceramic Society, 2007, 27, 3351-3357.	2.8	80
14	Novel analytical model for the determination of grain size distributions in nanocrystalline materials with low lattice microstrains by X-ray diffractometry. Acta Materialia, 2006, 54, 1-10.	3.8	72
15	Clarifying the effect of sintering conditions on the microstructure and mechanical properties of β-tricalcium phosphate. Ceramics International, 2010, 36, 1929-1935.	2.3	72
16	Additive-free superhard B4C with ultrafine-grained dense microstructures. Journal of the European Ceramic Society, 2014, 34, 841-848.	2.8	71
17	Densification of additive-free polycrystalline β-SiC by spark-plasma sintering. Ceramics International, 2012, 38, 45-53.	2.3	68
18	Crystal-size dependence of the spark-plasma-sintering kinetics of ZrB2 ultra-high-temperature ceramics. Journal of the European Ceramic Society, 2012, 32, 271-276.	2.8	68

#	Article	IF	CITATIONS
19	A route for the pressureless liquid-phase sintering of SiC with low additive content for improved sliding-wear resistance. Journal of the European Ceramic Society, 2012, 32, 965-973.	2.8	68
20	Effect of Microstructure on Slidingâ€Wear Properties of Liquidâ€Phaseâ€5intered αâ€5iC. Journal of the American Ceramic Society, 2005, 88, 2159-2163.	1.9	65
21	A direct comparison in the fatigue resistance enhanced by surface severe plastic deformation and shot peening in a C-2000 superalloy. Materials Science & Engineering A: Structural Materials: Properties, Microstructure and Processing, 2010, 527, 986-994.	2.6	64
22	Hall–Petch relationship in a nanotwinned nickel alloy. Scripta Materialia, 2008, 58, 951-954.	2.6	63
23	Experimental study of the microstructure and stress state of shot peened and surface mechanical attrition treated nickel alloys. Scripta Materialia, 2010, 62, 129-132.	2.6	63
24	Microstructural Evolution in Liquidâ€Phaseâ€Sintered SiC: Part I, Effect of Starting Powder. Journal of the American Ceramic Society, 2001, 84, 1578-1584.	1.9	61
25	Sliding-Wear-Resistant Liquid-Phase-Sintered SiC Processed Using ?-SiC Starting Powders. Journal of the American Ceramic Society, 2007, 90, 541-545.	1.9	61
26	Spark-plasma sintering of ZrB2 ultra-high-temperature ceramics at lower temperature via nanoscale crystal refinement. Journal of the European Ceramic Society, 2012, 32, 2529-2536.	2.8	58
27	Room temperature "one-pot―solution synthesis of nanoscale CsSnI3 orthorhombic perovskite thin films and particles. Materials Letters, 2013, 110, 127-129.	1.3	58
28	Oxidation behaviour of pressureless liquid-phase-sintered α-SiC with additions of 5Al2O3+3RE2O3 (RE=La, Nd, Y, Er, Tm, or Yb). Journal of the European Ceramic Society, 2010, 30, 3209-3217.	2.8	55
29	Fabricating geometrically-complex B4C ceramic components by robocasting and pressureless spark plasma sintering. Scripta Materialia, 2018, 145, 14-18.	2.6	50
30	X-ray powder diffraction analysis of a silicon carbide-based ceramic. Materials Letters, 2001, 49, 137-145.	1.3	48
31	Densification of B4C nanopowder with nanograin retention by spark-plasma sintering. Journal of the European Ceramic Society, 2015, 35, 1991-1998.	2.8	48
32	Effect of intergranular phase chemistry on the sliding-wear resistance of pressureless liquid-phase-sintered α-SiC. Journal of the European Ceramic Society, 2012, 32, 511-516.	2.8	46
33	Improved Sliding-Wear Resistance in In Situ-Toughened Silicon Carbide. Journal of the American Ceramic Society, 2005, 88, 3531-3534.	1.9	45
34	Effect of liquid-phase content on the contact-mechanical properties of liquid-phase-sintered α-SiC. Journal of the European Ceramic Society, 2007, 27, 2521-2527.	2.8	44
35	Crystallite Size Refinement of ZrB <sub>2</sub> by Highâ€Energy Ball Milling. Journal of the American Ceramic Society, 2009, 92, 3114-3117.	1.9	44
36	A comparative study of the tribological performance of ferrofluids and magnetorheological fluids within steel–steel point contacts. Tribology International, 2014, 78, 125-133.	3.0	43

#	Article	IF	CITATIONS
37	Stability of Lithium Hydride in Argon and Air. Journal of Physical Chemistry B, 2006, 110, 10567-10575.	1.2	42
38	Quantitative Phaseâ€Composition Analysis of Liquidâ€Phaseâ€Sintered Silicon Carbide Using the Rietveld Method. Journal of the American Ceramic Society, 2000, 83, 2282-2286.	1.9	41
39	Fabricating toughened super-hard B4C composites at lower temperature by transient liquid-phase assisted spark plasma sintering with MoSi2 additives. Journal of the European Ceramic Society, 2019, 39, 2862-2873.	2.8	41
40	Anomalous oxidation behaviour of pressureless liquid-phase-sintered SiC. Journal of the European Ceramic Society, 2011, 31, 2393-2400.	2.8	39
41	Tribological behavior of ionic liquid-based magnetorheological fluids in steel and polymeric point contacts. Tribology International, 2015, 81, 309-320.	3.0	39
42	Analytical formulation of the variance method of line-broadening analysis for Voigtian X-ray diffraction peaks. Journal of Applied Crystallography, 2006, 39, 598-600.	1.9	38
43	Effect of sintering atmosphere on the mechanical properties of liquid-phase-sintered SiC. Journal of the European Ceramic Society, 2004, 24, 3245-3249.	2.8	37
44	Tensile properties of a nickel-base alloy subjected to surface severe plastic deformation. Materials Science & Engineering A: Structural Materials: Properties, Microstructure and Processing, 2008, 493, 176-183.	2.6	37
45	Enhancing the sliding-wear resistance of SiC nanostructured ceramics by adding carbon nanotubes. Journal of the European Ceramic Society, 2016, 36, 3083-3089.	2.8	36
46	A Family of Hydrogels Based on Ureido‣inked Aminopolyolâ€Đerived Amphiphiles and Bolaamphiphiles: Synthesis, Gelation under Thermal and Sonochemical Stimuli, and Mesomorphic Characterization. Chemistry - A European Journal, 2008, 14, 5656-5669.	1.7	35
47	Fracture, fatigue, and sliding-wear behavior of nanocomposites of alumina and reduced graphene-oxide. Acta Materialia, 2020, 186, 29-39.	3.8	35
48	A study of the oxidation of ZrB2 powders during high-energy ball-milling in air. Ceramics International, 2012, 38, 2857-2863.	2.3	34
49	Liquid-phase assisted flash sintering of SiC from powder mixtures prepared by aqueous colloidal processing. Journal of the European Ceramic Society, 2017, 37, 485-498.	2.8	34
50	New acrylic monolithic carbon molecular sieves for O2/N2 and CO2/CH4 separations. Carbon, 2006, 44, 1158-1165.	5.4	33
51	On the crystallite size refinement of ZrB2 by high-energy ball-milling in the presence of SiC. Journal of the European Ceramic Society, 2011, 31, 2407-2414.	2.8	33
52	On the enhancement of the spark-plasma sintering kinetics of ZrB2–SiC powder mixtures subjected to high-energy co-ball-milling. Ceramics International, 2013, 39, 4191-4204.	2.3	33
53	Microstructural Evolution in Liquidâ€Phase‣intered SiC: Part III, Effect of Nitrogenâ€Gas Sintering Atmosphere. Journal of the American Ceramic Society, 2002, 85, 1835-1840.	1.9	31
54	Effect of sintering temperature on the microstructure and mechanical properties of ZrO2-3mol%Y2O3 sol–gel films. Ceramics International, 2010, 36, 2281-2286.	2.3	31

#	Article	IF	CITATIONS
55	Improvement of the Sparkâ€Plasmaâ€Sintering Kinetics of <scp><scp>ZrC</scp></scp> by Highâ€Energy Ballâ€Milling. Journal of the American Ceramic Society, 2012, 95, 453-456.	1.9	31
56	Sliding-wear resistance of liquid-phase-sintered SiC containing graphite nanodispersoids. Journal of the European Ceramic Society, 2014, 34, 2597-2602.	2.8	31
57	Liquid-phase assisted spark-plasma sintering of SiC nanoceramics and their nanocomposites with carbon nanotubes. Journal of the European Ceramic Society, 2017, 37, 1929-1936.	2.8	31
58	Textural and morphological study of activated carbon fibers prepared from kenaf. Microporous and Mesoporous Materials, 2008, 111, 523-529.	2.2	30
59	Near-net shape manufacture of B4C–Co and ZrC–Co composites by slip casting and pressureless sintering. Journal of the European Ceramic Society, 2017, 37, 4577-4584.	2.8	30
60	Sliding-wear resistance of ultrafine-grained SiC densified by spark plasma sintering with 3Y2O3+5Al2O3 or Y3Al5O12 additives. Scripta Materialia, 2013, 69, 598-601.	2.6	29
61	The prolific polytypism of silicon carbide. Journal of Applied Crystallography, 2013, 46, 242-247.	1.9	29
62	Highly sliding-wear resistant B4C composites fabricated by spark-plasma sintering with Ti–Al additives. Scripta Materialia, 2020, 177, 91-95.	2.6	28
63	Microstructural Evolution in Liquidâ€Phaseâ€Sintered SiC: Part II, Effects of Planar Defects and Seeds in the Starting Powder. Journal of the American Ceramic Society, 2001, 84, 1585-1590.	1.9	27
64	Microstructural effects on the sliding wear of transparent magnesium-aluminate spinel. Journal of the European Ceramic Society, 2012, 32, 3143-3149.	2.8	27
65	Comminution of B4C powders with a high-energy mill operated in air in dry or wet conditions and its effect on their spark-plasma sinterability. Journal of the European Ceramic Society, 2017, 37, 3873-3884.	2.8	27
66	Hardness degradation in liquid-phase-sintered SiC with prolonged sintering. Journal of the European Ceramic Society, 2007, 27, 3359-3364.	2.8	26
67	Highâ€Energy Ball Milling of ZrB <sub>2</sub> in the Presence of Graphite. Journal of the American Ceramic Society, 2010, 93, 3072-3075.	1.9	26
68	Effect of hexagonal-BN additions on the sliding-wear resistance of fine-grained α-SiC densified with Y3Al5O12 liquid phase by spark-plasma sintering. Journal of the European Ceramic Society, 2014, 34, 565-574.	2.8	26
69	In situ formation of ZrB2–ZrO2 ultra-high-temperature ceramic composites from high-energy ball-milled ZrB2 powders. Journal of Alloys and Compounds, 2012, 518, 38-43.	2.8	25
70	Contact-mechanical properties at pre-creep temperatures of fine-grained graphene/SiC composites prepared in situ by spark-plasma sintering. Journal of the European Ceramic Society, 2014, 34, 1433-1438.	2.8	25
71	Synthesis and photocatalytic activity of Eu3+-doped nanoparticulate TiO2 sols and thermal stability of the resulting xerogels. Materials Chemistry and Physics, 2014, 144, 8-16.	2.0	25
72	Aqueous colloidal processing of nano-SiC and its nano-Y3Al5O12 liquid-phase sintering additives with carbon nanotubes. Journal of the European Ceramic Society, 2015, 35, 3363-3368.	2.8	25

#	Article	IF	CITATIONS
73	Fundamental parameters approach in the Rietveld method: a study of the stability of results versus the accuracy of the instrumental profile. Journal of the European Ceramic Society, 2000, 20, 1845-1851.	2.8	24
74	Quantitative polytype-composition analyses of SiC using X-ray diffraction: a critical comparison between the polymorphic and the Rietveld methods. Journal of the European Ceramic Society, 2001, 21, 1237-1248.	2.8	24
75	Crystallite sizes of LiH before and after ball milling and thermal exposure. Journal of Alloys and Compounds, 2008, 454, 297-305.	2.8	24
76	Effect of MoSi2 content on the lubricated sliding-wear resistance of ZrC–MoSi2 composites. Journal of the European Ceramic Society, 2011, 31, 877-882.	2.8	24
77	CMAS-Resistant Plasma Sprayed Thermal Barrier Coatings Based on Y2O3-Stabilized ZrO2 with Al3+ and Ti4+ Solute Additions. Journal of Thermal Spray Technology, 2014, 23, 708-715.	1.6	23
78	Enhancing the spark-plasma sinterability of B4C nanopowders via room-temperature methylation induced purification. Journal of the European Ceramic Society, 2016, 36, 2843-2848.	2.8	23
79	Effect of the sintering additive content on the non-protective oxidation behaviour of pressureless liquid-phase-sintered l±-SiC in air. Journal of the European Ceramic Society, 2010, 30, 1513-1518.	2.8	22
80	Aqueous colloidal processing of SiC with Y3Al5O12 liquid-phase sintering additives. Journal of the European Ceramic Society, 2013, 33, 1685-1694.	2.8	22
81	Influence of the synthesis process on the features of Y2O3-stabilized ZrO2 powders obtained by the sol–gel method. Ceramics International, 2014, 40, 6421-6426.	2.3	22
82	Contact-mechanical properties at intermediate temperatures of ZrB2 ultra-high-temperature ceramics pressureless sintered with Mo, Ta, or Zr disilicides. Journal of the European Ceramic Society, 2015, 35, 3179-3185.	2.8	22
83	Reinforcement with reduced graphene oxide of bioactive glass scaffolds fabricated by robocasting. Journal of the European Ceramic Society, 2017, 37, 3695-3704.	2.8	22
84	Determination of the thermal stability and isothermal bulk modulus of the ZrO2 polymorphs at room temperature by molecular dynamics with a semi-empirical quantum-chemical model. Ceramics International, 2007, 33, 705-709.	2.3	21
85	Creep and Microstructural Evolution at High Temperature of Liquid-Phase-Sintered Silicon Carbide. Journal of the American Ceramic Society, 2007, 90, 163-169.	1.9	21
86	Effect of the nature of the intergranular phase on sliding-wear resistance of liquid-phase-sintered α-SiC. Scripta Materialia, 2007, 57, 505-508.	2.6	21
87	Rare earth-doped TiO2 nanocrystalline thin films: Preparation and thermal stability. Journal of the European Ceramic Society, 2014, 34, 4457-4462.	2.8	21
88	Transient liquid-phase assisted spark-plasma sintering and dry sliding wear of B4C ceramics fabricated from B4C nanopowders. Journal of the European Ceramic Society, 2021, 41, 1869-1877.	2.8	21
89	Complex impedance spectroscopy study of a liquid-phase-sintered α-SiC ceramic. Journal of the European Ceramic Society, 2007, 27, 3935-3939.	2.8	20
90	Structure determination of di-μ-hydroxo-bis[(2-(2-pyridyl)phenyl-κ2 N,C 1)palladium(II)] by X-ray powder diffractometry. Acta Crystallographica Section B: Structural Science, 2007, 63, 75-80.	1.8	20

#	Article	IF	CITATIONS
91	Effect of processing conditions on the sliding-wear resistance of ZrC triboceramics fabricated by spark-plasma sintering. Ceramics International, 2015, 41, 15278-15282.	2.3	20
92	Microstructural evolution and contact-mechanical properties of SiC ceramics prepared colloidally with low additive content. Ceramics International, 2012, 38, 5979-5986.	2.3	19
93	Spark-plasma-sintering kinetics of ZrC–SiC powder mixtures subjected to high-energy co-ball-milling. Ceramics International, 2013, 39, 9691-9697.	2.3	19
94	Spark plasma sinterability and dry sliding-wear resistance of WC densified with Co, Co+Ni, and Co+Ni+Cr. International Journal of Refractory Metals and Hard Materials, 2020, 92, 105280.	1.7	19
95	Improving the dry sliding-wear resistance of B4C ceramics by transient liquid-phase sintering. Journal of the European Ceramic Society, 2020, 40, 5286-5292.	2.8	18
96	Effect of the sintering additive content on the protective passive oxidation behaviour of pressureless liquid-phase-sintered SiC. Journal of the European Ceramic Society, 2012, 32, 3531-3536.	2.8	17
97	Microstructural effects on the sliding-wear resistance of pressureless liquid-phase-sintered SiC under diesel fuel. Journal of the European Ceramic Society, 2013, 33, 879-885.	2.8	17
98	Effect of graphite addition on the spark-plasma sinterability of ZrB2 and ZrB2–SiC ultra-high-temperature ceramics. Ceramics International, 2014, 40, 11457-11464.	2.3	17
99	Aqueous colloidal processing of near-net shape B 4 C–Ni cermet compacts. Journal of the European Ceramic Society, 2016, 36, 1915-1921.	2.8	17
100	Microstructural development during heat treatment of a commercially available dental-grade lithium disilicate glass-ceramic. Dental Materials, 2019, 35, 697-708.	1.6	17
101	Pressureless ultrafast sintering of near-net-shaped superhard isotropic B4C/rGO composites with Ti-Al additives. Journal of the European Ceramic Society, 2020, 40, 4354-4360.	2.8	17
102	Effect of Ar or N2 sintering atmosphere on the high-temperature oxidation behaviour of pressureless liquid-phase-sintered α-SiC in air. Journal of the European Ceramic Society, 2010, 30, 119-128.	2.8	16
103	Sliding-wear resistance of pure near fully-dense B4C under lubrication with water, diesel fuel, and paraffin oil. Journal of the European Ceramic Society, 2018, 38, 1158-1163.	2.8	16
104	Effect of high-energy ball-milling on the spark plasma sinterability of ZrB2 with transition metal disilicides. Journal of the European Ceramic Society, 2020, 40, 5020-5028.	2.8	16
105	Effect of calcination temperature on the textural properties of 3mol% yttria-stabilized zirconia powders. Journal of Non-Crystalline Solids, 2010, 356, 175-178.	1.5	15
106	Effect of Er3+ doping on the thermal stability of TiO2 nanoparticulate xerogels. Journal of Nanoparticle Research, 2013, 15, 1.	0.8	15
107	Aqueous colloidal processing of submicrometric SiC plus Y3Al5O12 with diamond nanoparticles. Journal of the European Ceramic Society, 2013, 33, 2473-2482.	2.8	15
108	Microstructural effects on the sliding-wear resistance of ZrC–MoSi 2 triboceramics fabricated by spark-plasma sintering. Journal of the European Ceramic Society, 2016, 36, 3091-3097.	2.8	15

#	Article	IF	CITATIONS
109	Structuralâ€Defectâ€Controlled Electrochemical Performance of Sodium Ion Batteries with NaCrO <sub>2</sub> Cathodes. ChemElectroChem, 2017, 4, 3222-3230.	1.7	15
110	Reinforcing 13–93 bioglass scaffolds fabricated by robocasting and pressureless spark plasma sintering with graphene oxide Journal of the Mechanical Behavior of Biomedical Materials, 2019, 97, 108-116.	1.5	15
111	Processing of orthotropic and isotropic superhard B4C composites reinforced with reduced graphene oxide. Journal of the European Ceramic Society, 2020, 40, 3406-3413.	2.8	15
112	Effect of type of solvent alcohol and its molar proportion on the drying critical thickness of ZrO2–3mol% Y2O3 films prepared by the sol–gel method. Surface and Coatings Technology, 2011, 205, 3540-3545.	2.2	14
113	Improving the sliding wear resistance of SiC nanoceramics fabricated by spark plasma sintering via gentle post-sintering annealing. Scripta Materialia, 2014, 77, 9-12.	2.6	14
114	Ceramics of Ta-doping stabilized orthorhombic ZrO2 densified by spark plasma sintering and the effect of post-annealing in air. Scripta Materialia, 2017, 130, 128-132.	2.6	14
115	Structural-microstructural characterization and optical properties of Eu3+,Tb3+-codoped LaPO4·nH2O and LaPO4 nanorods hydrothermally synthesized with microwaves. Ceramics International, 2018, 44, 11993-12001.	2.3	14
116	Manufacturing B4C parts with Ti-Al intermetallics by aqueous colloidal processing. Journal of the European Ceramic Society, 2020, 40, 226-233.	2.8	14
117	Ultra-low wear B4C-SiC-MoB2 composites fabricated at lower temperature from B4C with MoSi2 additives. Journal of the European Ceramic Society, 2021, 41, 68-75.	2.8	14
118	Structure determination of nitrato-lºO-bis[2-(2-pyridyl-lºN)amino-5,6-dihydro-4H-1,3-thiazine-lºN]copper(II) nitrateviamolecular modelling coupled with X-ray powder diffractometry. Journal of Applied Crystallography, 2004, 37, 993-999.	1.9	13
119	Oxidation behavior of pressureless liquid-phase-sintered α-SiC in ambient air at elevated temperatures. Journal of Materials Research, 2008, 23, 1689-1700.	1.2	13
120	Carbon nanotubes prevent the coagulation at high shear rates of aqueous suspensions of equiaxed ceramic nanoparticles. Journal of the European Ceramic Society, 2014, 34, 555-563.	2.8	12
121	Ultra-low temperature spark plasma sintering of super wear-resistant hard B4C composites. Scripta Materialia, 2022, 211, 114516.	2.6	12
122	Study of the Contributions of Non‣pecific and Specific Interactions during Fluoxetine Adsorption onto Activated Carbons. Clean - Soil, Air, Water, 2012, 40, 698-705.	0.7	11
123	Microwaveâ€assisted Hydrothermal Synthesis of Singleâ€crystal Nanorods of Rhabdophaneâ€type <scp><scp>Sr</scp></scp> a€doped <scp><scp>LaPO</scp></scp> 4· <i>n</i> <scp><scp>H<sub>2</sub>O</scp></scp> . Journal of the American Ceramic Society. 2014. 97. 750-758.	1.9	11
124	Influence of Nd3+ Doping on the Structure, Thermal Evolution and Photoluminescence Properties of Nanoparticulate TiO2 Xerogels. Journal of Alloys and Compounds, 2020, 819, 152972.	2.8	11
125	Enhancing the Electrochemical Performance of NaCrO2 through Structural Defect Control. ACS Applied Energy Materials, 2020, 3, 7216-7227.	2.5	11
126	A critical comparison of the tribocorrosive performance in highly-alkaline wet medium of ultrafine-grained WC cemented carbides with Co, Co+Ni, or Co+Ni+Cr binders. International Journal of Refractory Metals and Hard Materials, 2021, 95, 105452.	1.7	11

#	Article	IF	CITATIONS
127	Synthesis, molecular characterization by infrared spectroscopy, and crystal structure determination by X-ray powder diffractometry of [ZnCl2(TdTz)] [TdTz=2-(3,4-dichlorophenyl)imino-N-(2-thiazin-2-yl)thiazolidine]. Polyhedron, 2005, 24, 1975-1982.	1.0	10
128	X-ray line-broadening study of a liquid-phase-sintered silicon carbide. Journal of the European Ceramic Society, 2002, 22, 2677-2687.	2.8	9
129	Effect of N2 sintering atmosphere on the hardness of sol–gel films of 3mol% Y2O3-stabilized ZrO2. Thin Solid Films, 2010, 518, 2779-2782.	0.8	9
130	Hertzian Indentation of a ZrB <sub>2</sub> –30% SiC Ultraâ€Highâ€Temperature Ceramic up to 800°C in Air. Journal of the American Ceramic Society, 2010, 93, 1848-1851.	1.9	9
131	Microstructural development during crystallization firing of a dental-grade nanostructured lithia-zirconia glass-ceramic. Journal of the European Ceramic Society, 2021, 41, 5728-5739.	2.8	9
132	Ab initio structural determination of 2-(2-pyridyl)imino-N-(2-thiazolin-2-yl)thiazolidine from powder diffraction data. Materials Letters, 2004, 58, 672-678.	1.3	8
133	Effect of ion nitriding on the crystal structure of 3mol% Y2O3-doped ZrO2 thin-films prepared by the sol–gel method. Applied Surface Science, 2006, 252, 6018-6021.	3.1	8
134	Mechanical activation enhanced solid-state synthesis of NaCrO2 cathode material. Materialia, 2019, 5, 100172.	1.3	8
135	Bioinspired design of triboceramics: Learning from the anisotropic micro-fracture response of dental enamel under sliding contact. Ceramics International, 2020, 46, 27983-27989.	2.3	8
136	Fabrication of B4C ultrafiltration membranes on SiC supports. Journal of the European Ceramic Society, 2022, 42, 3118-3126.	2.8	8
137	Crystal structure of [NBu4]2[Pd2{C4(COOMe)4}2(μ-OH)2] determined ab initio by charge flipping. Journal of Alloys and Compounds, 2009, 467, 322-326.	2.8	7
138	Synthesis and structural characterization of two new copper(II) complexes with thiazoline derivative ligands: Influence of the coordination on the phagocytic activity of human neutrophils. Inorganica Chimica Acta, 2011, 365, 282-289.	1.2	7
139	Effect of Tb3+ doping and self-generated pressure on the crystallographic/morphological features and thermal stability of LaPO4A·nH2O single-crystal nanorods obtained by microwave-assisted hydrothermal synthesis. Ceramics International, 2016, 42, 18074-18086.	2.3	7
140	An in situ and ex situ study of the microstructural evolution of a novel lithium silicate glass-ceramic during crystallization firing. Dental Materials, 2020, 36, 645-659.	1.6	7
141	Fabrication of ultrafine-grained ZrC–Co cemented carbides with superior sliding-wear resistance from micrometre starting powders. Ceramics International, 2021, 47, 24831-24840.	2.3	7
142	Aqueous tape casting of super-hard B4C laminates with rGO-enriched reinforcing interlayers. Journal of the European Ceramic Society, 2021, 41, 5457-5465.	2.8	7
143	An analytical model for the determination of crystallite size andÂcrystal lattice microstrain distributions in nanocrystalline materials from the variance of the X-ray diffraction peaks. Applied Physics A: Materials Science and Processing, 2009, 94, 189.	1.1	6
144	Synthesis and structural characterization of two bond isomer copper(II) complexes via molecular modeling coupled with X-ray powder diffractometry. Polyhedron, 2011, 30, 1157-1162.	1.0	6

#	Article	IF	CITATIONS
145	A comparative study of the pressureless sinterability of 3 mol% Y 2 O 3 -stabilized ZrO 2 powders prepared by the sol–gel method under different synthesis conditions without modifiers. Ceramics International, 2014, 40, 16829-16834.	2.3	6
146	Processing and electrical conductivity of non-stoichiometric lanthanum strontium manganite perovskites prepared from powders synthesized by a polymerizable-complexation route. Ceramics International, 2018, 44, 13389-13395.	2.3	6
147	Some crystallographic considerations on the novel orthorhombic ZrO 2 stabilized with Ta doping. Ceramics International, 2018, 44, 10362-10366.	2.3	6
148	Effect of sintering duration on the slidingâ€wear resistance of 3Yâ€TZP dental ceramics. International Journal of Applied Ceramic Technology, 2019, 16, 1954-1961.	1.1	6
149	A comparative study of the dry sliding wear of WC-10wt.%(Co+Fe+Ni) cemented carbides pressureless sintered with different Fe/Co ratios. Journal of Asian Ceramic Societies, 2020, 8, 1043-1050.	1.0	6
150	Spark Plasma Sintering and Microstructural Characterization of Additive-Free Polycrystalline β-SiC. Key Engineering Materials, 0, 423, 67-72.	0.4	5
151	High-temperature compressive creep of novel fine-grained orthorhombic ZrO 2 ceramics stabilized with 12†mol% Ta doping. Journal of the European Ceramic Society, 2018, 38, 2445-2448.	2.8	5
152	Spark plasma sintering and dry sliding-wear of ZrC-16.7Âvol.% Co cemented carbides. Ceramics International, 2021, 47, 12803-12811.	2.3	5
153	Influence of Pr3+ doping on the synthesis of colloidal sols and nanoparticulate TiO2 xerogels and their photocatalytic activity. Materials Characterization, 2021, 182, 111536.	1.9	5
154	Synthesis, Spectroscopic Study and Crystal Structure Determination by Xâ€ray Powder Diffractometry of [CdCl <sub>2</sub> (TzTn)] [TzTn=2â€(3,4â€dichlorophenyl)iminoâ€Nâ€(2â€thiazolinâ€2â€yl)tetrahydroâ€1 Zeitschrift Fur Anorganische Und Allgemeine Chemie, 2007, 633, 1801-1808.	,3â€ <b>t</b> hiazi	ne¥.
155	An interplay between electronic and structural effects on the photoluminescence decay mechanisms in LaPO <sub>4</sub> · <i>n</i> H <sub>2</sub> O:Tb <sup>3+</sup> and LaPO <sub>4</sub> :Tb <sup>3+</sup> single-crystal nanorods. Journal of Materials Chemistry C, 2018, 6, 12643-12651.	2.7	4
156	Unraveling Processing-Structure-Electrical Conductivity Relationships of NaCrO2 Cathodes for Na-Ion Batteries. Journal of the Electrochemical Society, 2019, 166, A3546-A3553.	1.3	4
157	Influence of substrate and sintering temperature on the thickness and number of layers of 3YSZ multilayer sol-gel coatings. Ceramics International, 2020, 46, 18347-18351.	2.3	4
158	Effect of 1-D and 2-D carbon-based nano-reinforcements on the dry sliding-wear behaviour of 3Y-TZP ceramics. Journal of the European Ceramic Society, 2021, 41, 3595-3602.	2.8	4
159	Determination of Lattice Parameters of Polytypes in Liquidâ€Phaseâ€6intered SiC Using the Rietveld Method. Journal of the American Ceramic Society, 2004, 87, 943-949.	1.9	3
160	Discriminating between two chiral diastereoisomeric 7-oxanitronorbornenes by conventional X-ray powder diffractometry. Zeitschrift Für Kristallographie, 2010, 225, .	1.1	3
161	Effects of composition and crystallite size on the accuracy of the Rietveld method in determining lattice parameters of polytypes in multiphase SiC ceramics. Ceramics International, 2012, 38, 4285-4293.	2.3	3
162	Fabricating eco-friendly nanocomposites of SiC with morphologically-different nano-carbonaceous phases. Journal of the European Ceramic Society, 2018, 38, 3735-3741.	2.8	3

#	Article	IF	CITATIONS
163	A simple, accurate and effective polymorphic method to determine phase compositions of SiC-based ceramics. Journal of the European Ceramic Society, 2004, 24, 2885-2894.	2.8	2
164	A line-broadening analysis model for the microstructural characterization of nanocrystalline materials from asymmetric x-ray diffraction peaks. Journal of Physics Condensed Matter, 2012, 24, 215301.	0.7	2
165	Evaluating nanocrystallite size distributions in doped and undoped nanocrystalline ceramics by X-ray diffractometry. Ceramics International, 2018, 44, 22365-22369.	2.3	2
166	Aplicación del método de Rietveld al análisis cuantitativo SiC sinterizado en fase lÃquida. Boletin De La Sociedad Espanola De Ceramica Y Vidrio, 2000, 39, 347-350.	0.9	2
167	Determinación de la composición de fases en circona mediante un procedimiento polimórfico simple. Boletin De La Sociedad Espanola De Ceramica Y Vidrio, 2004, 43, 23-25.	0.9	2
168	Sliding-wear performance of ZrC–Co: A comparative assessment under dry and neutral/non-neutral wet media. Ceramics International, 2022, 48, 6880-6889.	2.3	2
169	Accuracy of X-ray diffraction SiC polytype-composition analyses performed by a polymorphic method. Journal of Materials Science Letters, 2001, 20, 297-299.	0.5	1
170	Evaluation of the phase composition of (NH4)2SO4+(NH4)H2PO4 mixtures by X-ray diffractometry. Journal of Alloys and Compounds, 2009, 475, 686-692.	2.8	1
171	Unexpected Reactions: From (2S,3R)-2-(endo-d-Galacto-pentaacetoxypentyl)-1,4-dimethyl-3-exo-nitro-7-oxabicyclo[2.2.1]hept-5-ene to Chiral Cyclic Ethers. Synlett, 2008, 2008, 687-690.	1.0	0